TISSUE ENGINEERING: Part A
Volume 00, Number 00, 2024

DOI: 10.1089/ten.tea.2024.0076

termis
Tissue Engineering
& Regenerative Medicine
International Society

Open camera or QR reader and scan code to access this article and other resources online.

ORIGINAL ARTICLE

Comparative Analysis of Commercially Available Extracellular Matrix Soft Tissue Bioscaffolds

Tarek Kollmetz, PhD,[1] Fernanda Castillo-Alcala, BVSc, DVS, Dip. ACVP,[2] Robert W. F. Veale, MBioEnt,[1] Navid Taghavi, PhD,[1] Vonne M. van Heeswijk, PhD,[3] Maarten Persenaire, MD,[4,†] Barnaby C. H. May, PhD,[1] and Sandi G. Dempsey, PhD[1]

Decellularized extracellular matrix (dECM) products are widely established for soft tissue repair, reconstruction, and reinforcement. These regenerative biomaterials mimic native tissue ECM with respect to structure and biology and are produced from a range of tissue sources and species. Optimal source tissue processing requires a balance between removal of cellular material and the preservation of structural and biological properties of tissue ECM. Despite the widespread clinical use of dECM products there is a lack of comparative information on these products. This study provides a comparative analysis of 12 commercially available dECM products. One group of products consisted of materials intended for dermal repair including ovine forestomach matrix (OFMm), porcine peritoneum (PPN), porcine placenta (PPC), and porcine small intestinal submucosa (SISu). The second group, intended for load-bearing reconstruction, consisted of material derived from ovine forestomach matrix (OFMo), porcine urinary bladder matrix (UBM), porcine small intestinal submucosa (SISb and SISz), human dermis (ADM), porcine dermis (PADM), and fetal/neonatal bovine dermis (BADM). A minimally processed product consisting of human placental tissue was included as a control. Products were compared histologically and by agarose gel electrophoreses to assess structural features and decellularization. Structurally, some dECM products showed a well-preserved collagen architecture with a broad porosity distribution, whereas others showed a significantly altered structure compared with native tissue. Decellularization varied across the products. Some materials surveyed (OFMm, PPN, PPC, OFMo, UBM, SISz, ADM, PADM, and BADM) were essentially devoid of nuclear bodies (mean count of <5 cells per high-powered field [HPF]), whereas others (SISu and SISb) demonstrated an abundance of nuclear bodies (>50 cells per HPF). Pathology assessment of the products demonstrated that OFMm, OFMo, and PADM had the highest qualitative assessment score for collagen fiber orientation and arrangement, matrix porosity, decellularization efficiency, and residual vascular channels scoring 10.5 ± 0.8, 12.8 ± 1.0, and 9.7 ± 0.7 out of a maximum total score of 16, respectively. This analysis of commercially available dECM products in terms of their structure and cellularity includes 12 different commercial materials. The findings highlight the variability of the products in terms of matrix structure and the efficacy of decellularization.

Keywords: ovine forestomach matrix, tissue repair, plastics and reconstructive surgery, extracellular matrix, bioscaffold

[1]Aroa Biosurgery Limited, Auckland, New Zealand.
[2]School of Veterinary Science, Massey University, Palmerston North, New Zealand.
[3]Chemical and Materials Engineering, University of Auckland, Auckland, New Zealand.
[4]Tela Bio Inc., Malvern, Pennsylvania, USA.
[†]Deceased.

Impact Statement

The comparative analysis of 12 commercially available decellularized extracellular matrix (dECM) products reveals a spectrum of structural integrity and decellularization efficacy crucial for soft tissue repair and reconstruction. Although some dECM materials exhibit well-preserved collagen architecture and minimal cellularity, others display significant alterations and residual cellular components. Notably, products derived from ovine forestomach matrix, porcine peritoneum, and porcine placenta demonstrate optimal decellularization and structural fidelity, promising improved clinical outcomes. This study underscores the imperative for comprehensive assessments of dECM products, shedding light on their variable quality and potential implications for tissue regeneration. Such insights lay the groundwork for informed clinical decision-making and advancements in regenerative medicine.

Introduction

Soft tissue loss resulting from trauma, surgical intervention, or disease presents a continuing challenge in modern surgery, requiring reconstruction, regeneration, or reinforcement.[1,2] Primary closure or free, regional, and local tissue flaps are still considered the gold standard for reconstruction.[3] However, in instances where available tissue is limited, or less complex procedures are preferred, engineered bioscaffolds fill an immediate surgical need. Bioscaffolds represent the intersection of regenerative medicine, tissue engineering, and biomaterials science and aim to restore tissue function and improve patient outcomes by providing ready-to-use devices that can be deployed across a range of soft tissue reconstruction procedures. Bioscaffolds are now routinely used across a range of soft tissue reconstruction procedures, being applied both topically (e.g., partial and full thickness cutaneous wounds) and as implants (e.g., ventral hernia repair) to reinforce soft tissues in load-bearing applications. The last two decades have seen a rise in the number of commercially available regenerative bioscaffolds available for soft tissue repair and regeneration.[4] Structurally, these products act as a temporary scaffold to assist the healing process by scaffolding cellular infiltration, migration and proliferation while providing protection and reinforcement until the bioscaffold is ultimately assimilated into the regenerating tissues.[5]

In living tissue, the extracellular matrix (ECM) guides growth, maintains homeostasis and promotes repair after damage.[6] Tissue ECM is composed of a dynamic environment undergoing structural and biochemical modifications in a process known as "dynamic reciprocity."[7] As a novel approach to the preparation of bioscaffolds, decellularized ECMs (dECM), first posited by Badylak and colleagues in 1995,[8] make use of isolated tissue ECM as a bioactive scaffold for soft tissue repair procedures. The creation of dECMs involves removal of cells and cellular debris from a source tissue while preserving the structure and biology of the tissue ECM. Tissue decellularization yields a natural, biocompatible bioscaffold that is imbued with regenerative properties, including native architecture and biology, in the form of naturally occurring ECM components such as glycosaminoglycans and growth factors. This "top-down" approach to bioscaffold preparation contrasts with the bottom-up approach to synthetic bioscaffolds.

Commercially available dECM bioscaffolds are manufactured from various tissue sources including porcine small intestine, porcine urinary bladder, ovine forestomach, and human, bovine, and porcine dermis.[9] The manufacture of dECM-based devices is a careful balance between effective decellularization and retention of tissue ECM structure and biology. Effective removal of cells and cellular debris reduces the risk of an immune response.[10,11] Decellularization reagents (e.g., detergents, chelating agents), method of sterilization (e.g., radiative, ethylene oxide), and lyophilization methods are all known to impact the quality of the resulting dECM.[12] The choice of source tissue and age of the donor also plays a role in the structural and biological properties of the dECM.[12] For example, donor tissue age has been shown to influence degradation kinetics, thermal stability, and cell binding.[13–15]

Commercially available dECM devices are widely utilized across a range of in-patient and out-patient procedures, including peridontal, vascular, orthopedic, general, plastic, and reconstructive surgery, and for burns and wound care.[16–18]

The test articles in this study are derived from a variety of sources including ovine forestomach matrix (OFMm and OFMo), porcine peritoneum (PPN), porcine placenta (PPC), porcine small intestinal submucosa (SISu, SISb, and SISz), human dermis (ADM), porcine dermis (PADM), and bovine neonatal dermis (BADM). All the materials in the study are noncrosslinked; however, OFMo, SISb, and SISz contain additional polymers (see Table 1). Different dECM bioscaffolds such as UBM, OFM, or SIS are available in different formats, designed for specific applications, and leading to various commercial products derived from the same dECM technology. SIS-based materials were the earliest dECMs to be commercialized, thus a wealth of scientific and clinical literature sits behind this technology[19–23] with the pioneering study being published in 1989.[24] OFM has been widely reported in the scientific and clinical literature.[25–32] Scientific papers describing this technology have reported the composition,[31] bioactivity,[33] and structural "nativity" of the dECM in relation to unprocessed tissue.[25] Scientific literature around porcine urinary bladder matrix (UBM) is also abundant, with a particular focus on the composition, with a comprehensive proteomic analysis of UBM presented in 2017.[34] ADM materials (human, porcine, and neonatal), specifically the human-derived products, have been well researched in clinical literature.[35] Macroscopically, all the materials in this study have an off-white papery appearance, and this is demonstrated in Figure 1 with an image of OFMm.

There is a large amount of published research on the different dECM-based products used in this study, especially in relation to the biology of these materials. However, despite widespread usage, there is a dearth of comparative information

Table 1. Commercial Decellularized Extracellular Matrix Products Used in the Study

Product	*Manufacturer*	*Type*	*Tissue source*	*Additional components*	*Sterilization method*
Dermal reconstruction					
Myriad Matrix™	Aroa Biosurgery Limited (New Zealand) www.aroa.com	OFMm	Ovine forestomach	—	Ethylene oxide
Puracol® Ultra	Viscus Biologicals LLC (CA, United States) www.viscusbiologics.com	PPN	Porcine peritoneal	—	Gamma irradiation
InnovaMatrix®	ConvaTec (Reading, UK) www.convatec.com	PPC	Porcine placenta	—	Electron beam
OaSIS® Ultra	Cook Medical LLC (IN, United States) www.cookmedical.com	SISu	Porcine small intestinal submucosa	—	Ethylene oxide
Load-Bearing Reconstruction					
OviTex®	Aroa Biosurgery Limited (New Zealand) www.aroa.com	OFMo	Ovine forestomach	PGA or PP	Ethylene oxide
Gentrix®	ACell Inc. (MD, USA) www.integralife.com	UBM	Porcine bladder	—	Electron beam
Biodesign®	Cook Medical LLC (IN, United States) www.cookmedical.com	SISb	Porcine small intestinal submucosa	+/–PGA	Ethylene oxide
Zenapro®	Cook Medical LLC (IN, United States) www.cookmedical.com	SISz	Porcine small intestine submucosa	PP	Ethylene oxide
Alloderm™	Allergan Inc (NJ, United States) www.abbvie.com	ADM	Human dermis	—	Aseptically processed
Strattice™	Allergan Inc (NJ, United States) www.abbvie.com	PADM	Porcine dermis	—	Electron beam
SurgiMend®	Integra Lifesciences Corp (NJ, United States) www.integralife.com	BADM	Fetal/neonatal bovine dermis	—	Ethylene oxide
Minimally Processed Product					
EpiFix®	Mimedix (GA, United States) www.mimedx.com	HDAM	Human amnion/chorion	—	Electron beam

PGA, poly(glycolic acid); PP, polypropylene.

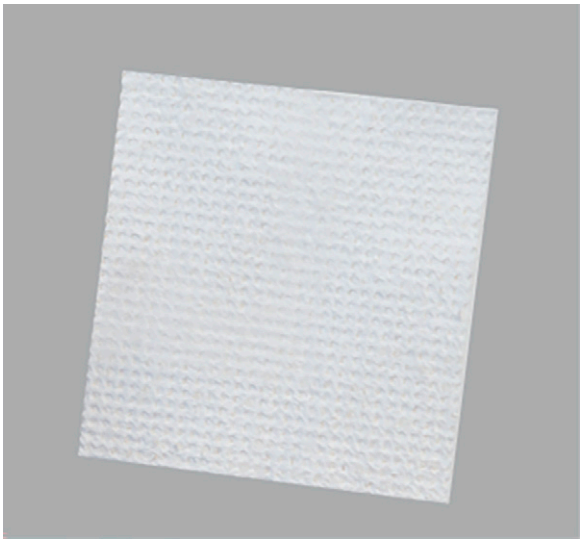

FIG. 1. Representative image of dECM biomaterial device intended for soft tissue repair. OFMm is a multilaminate decellularized material derived from ovine forestomach matrix with an off-white papery appearance. dECM, decellularized extracellular matrix; OFM, ovine forestomach matrix.

on these commercial dECM-based devices, specifically structural and process related phenomena, such as decellularization. To fill this knowledge gap, a comparative analysis was undertaken to assess structural features, and the relative decellularization of commercial dECM products.

Materials and Methods

General

Samples of products were obtained from commercial sources (Table 1). Samples of native tissues were included as reference samples and were collected from animals which had died from natural causes, tissue was collected less than 1 h after time of death and fixed in formalin at time of collection before transport to the lab. A slide containing human reference tissue was kindly supplied form the pathology lab Auckland University School of Medicine. All results were calculated as mean ± standard deviation (SD). Statistical significance was determined via one-way ANOVA, where "****" $p < 0.0001$, "***" $p < 0.001$, "**" $p < 0.01$, "*" $p < 0.1$, "ns" $p \geq 0.1$ using GraphPad Prism (Version 9.3.0, GraphPad Software, United States). Statistical tables are presented as Supplementary Material (Tables S1 and S2).

Image analysis

For the quantitative analyses, all results were calculated as mean ± standard deviation (SD). For image analysis, pieces of test article (>1 cm^2) were fixed and sectioned. Two sequential sections of each material were mounted on one slide, images were taken at evenly spaced intervals across both sections to give the number of technical replicates (number of high-powered field [HPF] images) for each measure. Nuclear bodies and diffuse staining: five images of each material from one slide (five technical replicates from one sample). For the pathology analysis, eight HPV images from two separate pieces of material were processed onto two slides and total of eight HPVs (four technical replicates from two samples) were scored. All results were calculated as mean ± standard deviation (SD) from the total number of measurements. For the agarose gel visual analysis (qualitative analysis) the results show a representative image from three separate experiments. Porosity is displayed via a representative image taken from one of the five images captured from the cross section of one piece of material.

Histological assessment

Samples were processed, stained, and imaged for histological analysis to compare and score metrics related to the physical structures and level of decellularization of the ECM cross-sections. Product samples were rehydrated in phosphate buffered saline (PBS) for 30 min. Product samples and reference tissue samples were fixed in 10% neutral buffered formalin (Sigma Aldrich, United States) for 24 h at room

TABLE 2. PATHOLOGY SCORING

Score	*1*	*2*	*3*	*4*
Collagen fiber arrangement and orientation	Fibers are compacted, fused, or otherwise damaged	Fiber arrangement is largely planar and substantially impacted by processing	Fiber arrangement is more three-dimensional though visibly impacted by processing	Fiber arrangement and orientation resembles native architecture
Matrix porosity	Tissue cross section is dense with no pores	Tissue cross section is relatively dense but demonstrates some isolated or sporadic pores	Tissue cross section is largely porous but lacks interconnected openings	Tissue cross section is porous with interconnected channels and openings
Cellular removal	Large number of cells and/or evidence of diffuse nuclear staining (>10 per HPF)	5–10 per HPF	1–5 per HPF	No cells per HPF nor evidence of diffuse nuclear staining
Residual vascular channels	Zero vascular channels per HPF	1–2 per HPF	3–4 per HPF	>5 vascular channels per HPF

HPF, high-powered field.

temperature followed by ethanol gradient dehydration and paraffin embedding, then oriented to give a cross-sectional area on the block face. Blocks were cut to 10-μm sections and mounted on slides giving two sections, each measuring ~10 mm in length per slide with two slides per sample. One slide of each product and reference sample were deparaffinized, hydrated and stained with hematoxylin and eosin (H&E), (Sigma-Aldrich, United States). A second slide of each product sample was deparaffinized, hydrated, and mounted in 4',6-diamidino-2-phenylindole (DAPI) Prolong™ Gold (Life Technologies, United States) mounting media.

Visual comparison of structure and porosity was performed because these inherent properties of the source ECM tissue impacts the rate of cellular infiltration when materials are used clinically. Cross sections stained with H&E were imaged at 63× and 25× magnification on an Axio Imager Z2 microscope (Zeiss, Germany) and a CoolCube 4 m (MetaSystems, Germany) camera equipped with a VSlide scanner (MetaSystems, Germany). The individual images were exported through VSViewer (Version 2.1.139, MetaSystems, Germany).

DAPI staining was performed in order to determine the relative levels of remaining cells and DNA. Cell counts for cross sections were performed to provide a visual estimate of the number of intact cells remaining in the cross section, while "diffuse staining" measured the area of the cross section that stained positive for DAPI to show the level of remnant extracellular DNA (rather than a distinct nuclei). DAPI-stained product samples were imaged using an Axio microscope and camera setup (Zeiss, Germany) using Metamorph software (Molecular Devices, United States) for image acquisition.

Nuclear bodies were manually counted from magnified (63×) DAPI images (five HPFs per sample) using ImageJ. Images were opened with the manual "counter" tool in ImageJ to give the total cell counts per HPF. The operator was trained to determine the size of a "cell" using the minimally processed control as a reference for the size and circularity of a mammalian cells at the magnification used. Images were coded to reduce operator bias.

Diffuse staining was quantified using the total area of signal detected for each image using "Analyze Particles" tool in ImageJ. RBG color images were converted to 8-bit images and the threshold was adjusted to 80% of the min and max for each image. The entire tissue section was selected and analyzed using the ImageJ "measure." The relative DAPI positive area was expressed as the total area of staining across the HPFQ7.

Agarose gel electrophoresis

Samples were enzymatically digested and run on an agarose gel in order to visualize the relative quantity of DNA in each sample. Product samples (50 mg) were digested in 1 mL papain (≥10 U/mg, Sigma Aldrich, United States, 0.5 mg/mL in papain buffer; 1× PBS, 1 M sodium chloride, 5 mM cysteine hydrochloride, 1.3 mM ethylenediaminetetraacetic acid) at 65°C for 22.5 h. Digested samples were centrifuged at 16000 *g* for 10 min, the supernatant was decanted, and DNA was precipitated in a mixture of sodium acetate (3 M, pH 5.2) and ice-cold ethanol (Sigma Aldrich, United States) at a supernatant/sodium acetate/ethanol volume ratio of 1/0.1/2.5 (350/35/875 μL). The mixtures were stored at −20°C for 22 h and subsequently centrifuged at 14000 g for 15 min. The supernatant was discarded, and the pellets were washed twice with 1 mL of 70% ethanol. Subsequently, the pellets were dried and resolubilized in 100 μL of reverse osmosis (RO) water. A DNA standard (12 μL of RO water, 1.5 μL of 10× BlueJuice loading buffer [Life Technologies, United States] and 1.5 μL of DNA ladder; 750 ng, 100–15,000 bp, Life Technologies, United States) was included on all gels. The DNA standard and products were loaded on a 1% E-Gel with SYBR Safe DNA gel stain (Life Technologies, United States) and run for 24 min in E-Gel Safe Imager Real-time Transilluminator (Life Technologies, United States). Gels were imaged on the E-Gel Safe Imager Real-time Transilluminator using a Nex-3N (Sony, Japan) digital camera equipped with a SELP1650 (Sony, Japan) interchangeable lens.

Pathology assessment

Pathology assessment was included in the analysis as a means to determine the relative native structure by the decellularized products, as well as the degree of decellularization. H&E-stained sections of each product sample (8 HPF/product) were reviewed by a U.S. board-certified veterinary pathologist (F.C-A.) and analyzed for degree of collagen fiber orientation and arrangement, presence of cellular bodies and residual DNA and residual vascular channels. Samples were coded such that the pathologist was blinded to the identification of product samples. Samples were scored according to Table 2, with the total score expressed out of maximum of 16.

Results

Collagen structure and porosity

To compare products with similar clinical indications, commercial devices in this study have been categorized under the general terms "dermal reconstruction" or "load-bearing reconstruction" (e.g., hernia repair). Representative H&E-stained images of unprocessed tissue were included as a qualitative reference to assess the impact of processing on the structure of dECM products. Unprocessed tissue samples include OFM, ovine peritoneum, ovine amnion/chorion, ovine bladder, porcine SIS, and bovine dermis (Figs. 2 and 3). HDAM (Fig. 2), a dehydrated human amnio/chorion membrane, was included in the panel as representative of a "minimally processed" product, in order to demonstrate an intact ECM with numerous cellular bodies present.

Representative H&E images of product samples are provided in Figure 2 (dermal reconstruction products) and Figure 3 (load-bearing reconstruction products). The samples presented a wide cross section of possible fiber arrangements. Some samples, for example OFMm (Fig. 2B and D), OFMo (Fig. 3B and D), and ADM (Fig. 3T and V) had an open architecture, with fibers of a variety of thicknesses. PADM (Fig. 3X and Y) was relatively dense, but the fiber staining resembled that of classical basket weave structure and resembling native dermis. The structure of BADM (Fig. 3AA and BB) was unique in the group, consisting of large pores, with fibers appearing less as discrete fibers but more as "sheets" and the overall structure did not resemble dermal ECM. PPN (Fig. 2G and I), UBM (Fig. 3G and I), SISu (Fig. 2L and N), and SISb (Fig. 3L and N) comprised layers of ECM. Rather than fibrous ECM, the architecture appeared compacted into

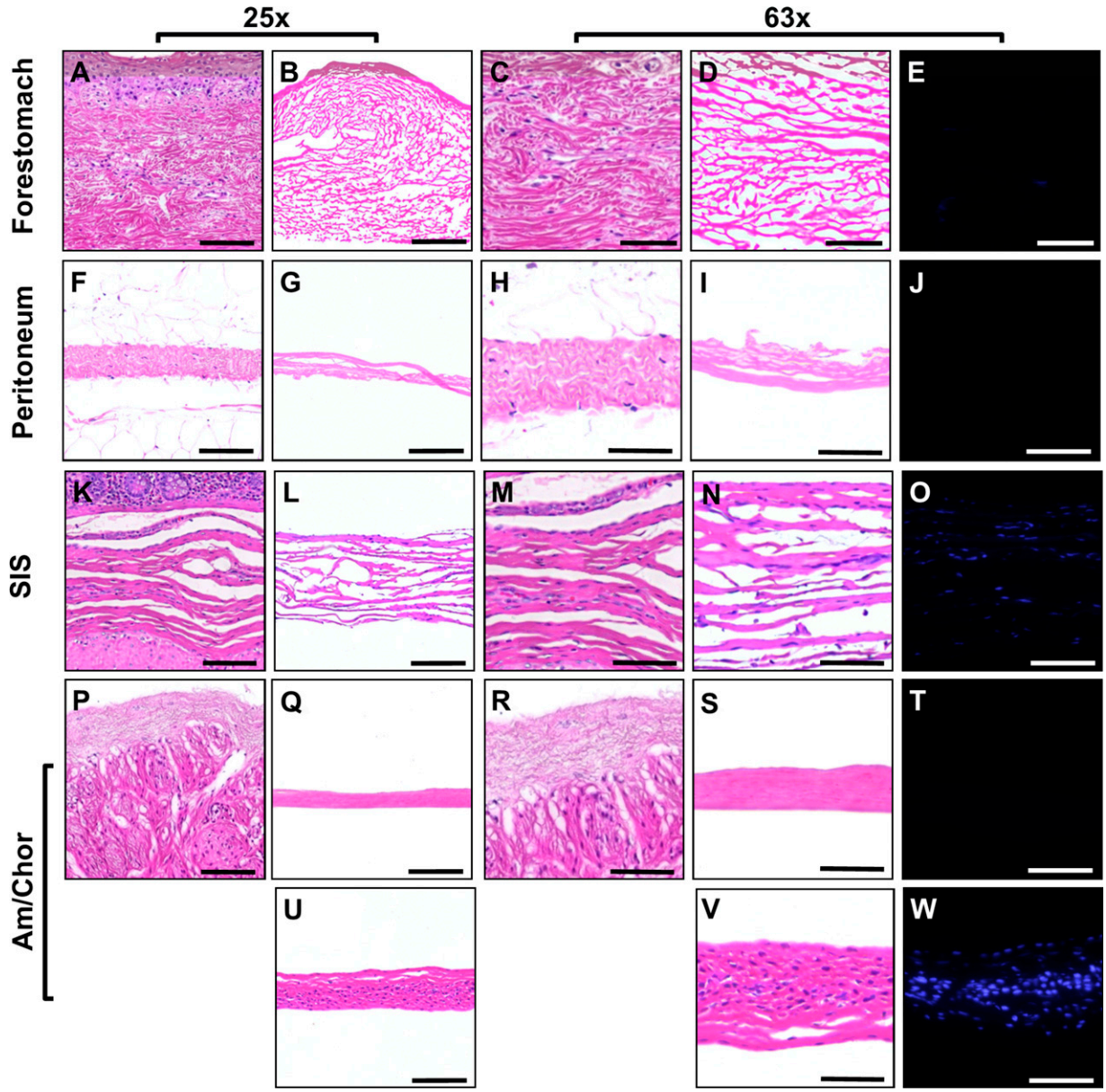

FIG. 2. Representative images of unprocessed reference tissue and dermal reconstruction products at 25× and 63× magnification. H&E-stained unprocessed forestomach tissue **(A)** and **(C)**; OFMm; **(B)** and **(D)** and DAPI-stained OFMm **(E).** H&E-stained unprocessed peritoneum tissue **(F)** and **(H)** PPN **(G)** and **(I)** and DAPI-stained PPN **(J).** H&E-stained unprocessed small intestinal submucosa tissue **(K)** and **(M)**; SISu **(L)** and **(N)** and DAPI-stained SISu **(O).** H&E-stained unprocessed amnion/chorion tissue **(P)** and **(R)**; PPC **(Q)** and **(S)** and DAPI-stained PPC **(T).** Amnion/chorion derived, minimally processed control HDAM was included as a reference, stained with H&E **(U)** and **(V)** and DAPI in **(W).** The scale bars of 25× images are 100 μm and the 63× images are 50 μm. DAPI, 4′,6-diamidino-2-phenylindole; H&E, hematoxylin and eosin; PPC, porcine placenta; PPN, porcine peritoneum.

layers of fused fibers with no discrete structure. Consequently, there were few or no pores within the matrices, and voids between adjacent sheets. SISz (Fig. 3P and Q) and PPC (Fig. 2Q and S) appeared as a dense single layer of ECM, essentially devoid of pores. Closer examination of the SISz (Fig. 3P and Q) revealed multiple layers of ECM that have been fused or compacted into a single layer of material. These findings are clearly observed in the inverted images of these sections showing a high level or absence of porosity in the materials (Fig. 4). PPC and SISz display a marked absence of pores (Fig. 4D and I) compared with other materials, whereas BADM (Fig. 4L) displayed a unique porosity pattern of larger pores than other materials.

Decellularization

DNA present in the product samples appeared either as part of discrete nuclear bodies, or as diffuse staining (Fig. 5). As expected, DNA in the minimally processed product, HDAM, predominantly stained as punctate cellular bodies, present throughout the material (Fig. 2W). ADM was absent of punctate staining but instead stained diffusely (Fig. 3W),

with nuclear material localized to the collagen fibers. SISu, UBM, and SISb had a high number of punctate cellular bodies throughout the material, evident in both H&E and DAPI stained samples (Fig. 2L, N, O; Fig. 3G, I, J, L, N, O). OFMm (Fig. 2B, D, E), PPN (Fig. 2G, I, J), PPC (Fig. 2Q, S, T), OFMo (Fig. 3B, D, E), PADM (Fig. 3X, Y, Z), and BADM (Fig. 3AA, BB, CC) were essentially devoid of nuclear material via visual inspection of the DAPI stained sections. These observations were confirmed via quantitative methods (Fig. 6 and Table 3). OFMm, OFMo, PPN, PPC, and SISz had on average less than one punctate nuclear body per HPF (Table 3). UBM, PADM, and BADM had approximately 1–5 per HPF; SISu and SISb had an abundance of DAPI positive nuclear bodies (>50 per HPF) (Table 3). Statistical analyses of these results are shown in Supplementary Table S2, demonstrating the means and variance between counts from images taken from one cross section.

DNA content via agarose gel electrophoresis

Double-stranded DNA present in the product samples was also analyzed through agarose gel electrophoresis. As expected, the minimally processed product, HDAM, exhibited intense broad bands of DNA ranging from 100 bp to more than 15000 bp. OFMm, OFMo, PPN, and PPC showed very subtle banding ranging from 100 bp to 300 bp (Fig. 6). UBM, SISu, and SISb also showed intense broad bands ranging from 100 bp to approximately 3000 bp with a localized high intensity band at approximately 300 bp. SISz showed a pronounced band ranging from approximately 100 bp to 500 bp. ADM exhibited an intense broad band from approximately 500 bp to more than 15000 bp, whereas PADM and BADM showed no detectable DNA bands. The results from DNA analysis via agarose gel were in agreement with the findings from DAPI stained product samples. Products that showed little detectable DAPI staining, that is, OFM representative for OFMo and OFMm, PPN, PPC, PADM, and BADM also showed little to no DNA present via agarose gel electrophoresis. Conversely, products that exhibited DAPI-positive staining (UBM, SISu, SISb, SISz, and ADM) showed DNA via agarose gel.

Pathology evaluation

Pathology scoring of dECM samples is shown in Table 4. and Figure 7. All dECM grafts presented prominent eosinophilic collagen structures. However, differences in collagen architecture preservation, degree of matrix porosity, and residual nuclear material were readily apparent between product samples.

PPN, SISu, SISz, and BADM all demonstrated damage to the collagen structure, with these products scoring 1.00 ± 0.00 in collagen fiber arrangement and orientation. This was mainly characterized by compact and fragmented collagen with little to no distinguishable individual fibers. OFMm, OFMo, and PADM exhibited the highest mean scoring for collagen structure (2.50 ± 0.53, 3.50 ± 0.53 and 2.88 ± 0.35, respectively), with distinguishable collagen fibers arranged in various directions and minimal disruption/damage of fibers.

Some products were relatively dense and nonporous, with PPN and SISz exhibiting the lowest score of 1.00 ± 0.00 with very dense and compact sheets. OFMm, OFMo, and BADM demonstrated the highest mean porosity score (3.38 ± 0.52, 3.88 ± 0.35 and 2.75 ± 0.46, respectively) where the materials were characterized by an evenly distributed porous structure. However, where OFMo and OFMm exhibited interconnected channels between pores in the material, BADM, while appearing porous, lacked interconnections between pores and channels.

Results of cellular removal assessment (decellularization) were highly variable. UBM, SISu, and SISb were found to contain marked residual cellular debris, all scoring 1.00 ± 0.00 and well-defined nuclear staining and/or substantial diffuse staining of nuclear chromatin. SISz also demonstrated residual cellularity, scoring 1.25 ± 0.46, but nuclear staining was pale relative to the well-defined staining of the aforementioned samples. The minimally processed product HDAM, as expected, had a well-preserved superficial layer lined by cells present on one side of the material. All other products were found to be largely devoid of remnant cellular material.

Assessment of residual vascular channels was the least variable measurement between product samples, with OFMo, UBM, SISz, and PADM sharing the highest score of 1.63 ± 0.52. Cumulative means of all pathological grading endpoints showed that the top three highest scoring products were OFMo, OFMm, and PADM with total mean scores of 12.8 ± 1.0, 10.5 ± 0.8, and 9.6 ± 0.7, respectively. All three of these devices had similar scores in all grading categories except porosity, where the structure of PADM was notably dense. Statistical analyses of these data are presented in Supplementary Table S1. The parallel processing of the samples and de-identification of samples in this analysis lowered the risk of bias from the pathologist. In addition, multiple samples from different devices of the same material were used in this analysis, so that the introduction of artifacts to the tissue processing would have shown as an outlier in the pathology scores.

Discussion

In this study, 12 commercially available dECM products with indications for dermal reconstruction and load-bearing reconstruction (e.g., hernia repair) were compared based on their structural properties and decellularization. These dECM products were selected based on their established use and popularity in these fields and their availability to the researchers at

FIG. 3. Representative images of unprocessed reference tissue and dermal reconstruction products at 25× and 63× magnification. H&E-stained unprocessed forestomach tissue **(A)** and **(C)**; OFMo; **(B)** and **(D)** and DAPI-stained OFMo **(E).** H&E-stained unprocessed bladder tissue **(F)** and **(H)**; UBM **(G)** and **(I)** and DAPI-stained UBM **(J).** H&E-stained unprocessed small intestinal submucosa tissue **(K)** and **(M)**; SISb **(L)** and **(N)** and DAPI-stained SISb **(O).** H&E-stained SISz **(P)** and **(Q)** and DAPI-stained SISz **(R).** H&E-stained unprocessed dermis tissue **(S)** and **(U)**; ADM **(T)** and **(V)** and DAPI-stained ADM **(W).** H&E-stained PADM **(X)** and **(Y)** and DAPI-stained PADM **(Z).** H&E-stained BADM **(AA)** and **(BB)** and DAPI-stained BADM **(CC).** The scale bars of 25× images are 100 μm and the 63× images are 50 μm. UBM, porcine urinary bladder matrix; ADM, human dermis; PADM, porcine dermis; BADM, fetal/neonatal bovine dermis.

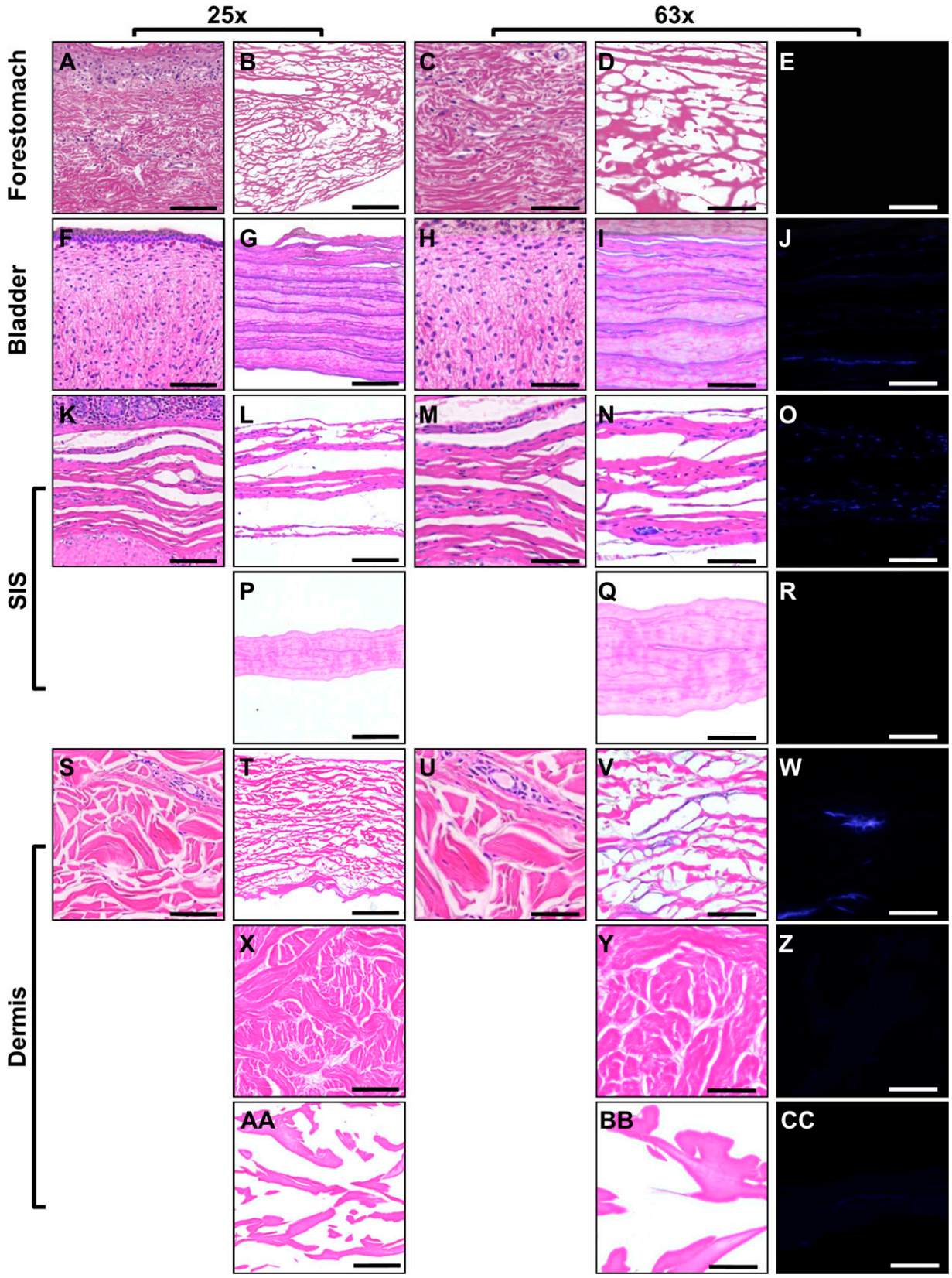
25x
63x
Forestomach
Bladder
SIS
Dermis
A
B
C
D
E
F
G
H
I
J
K
L
M
N
O
P
Q
R
S
T
U
V
W
X
Y
Z
AA
BB
CC

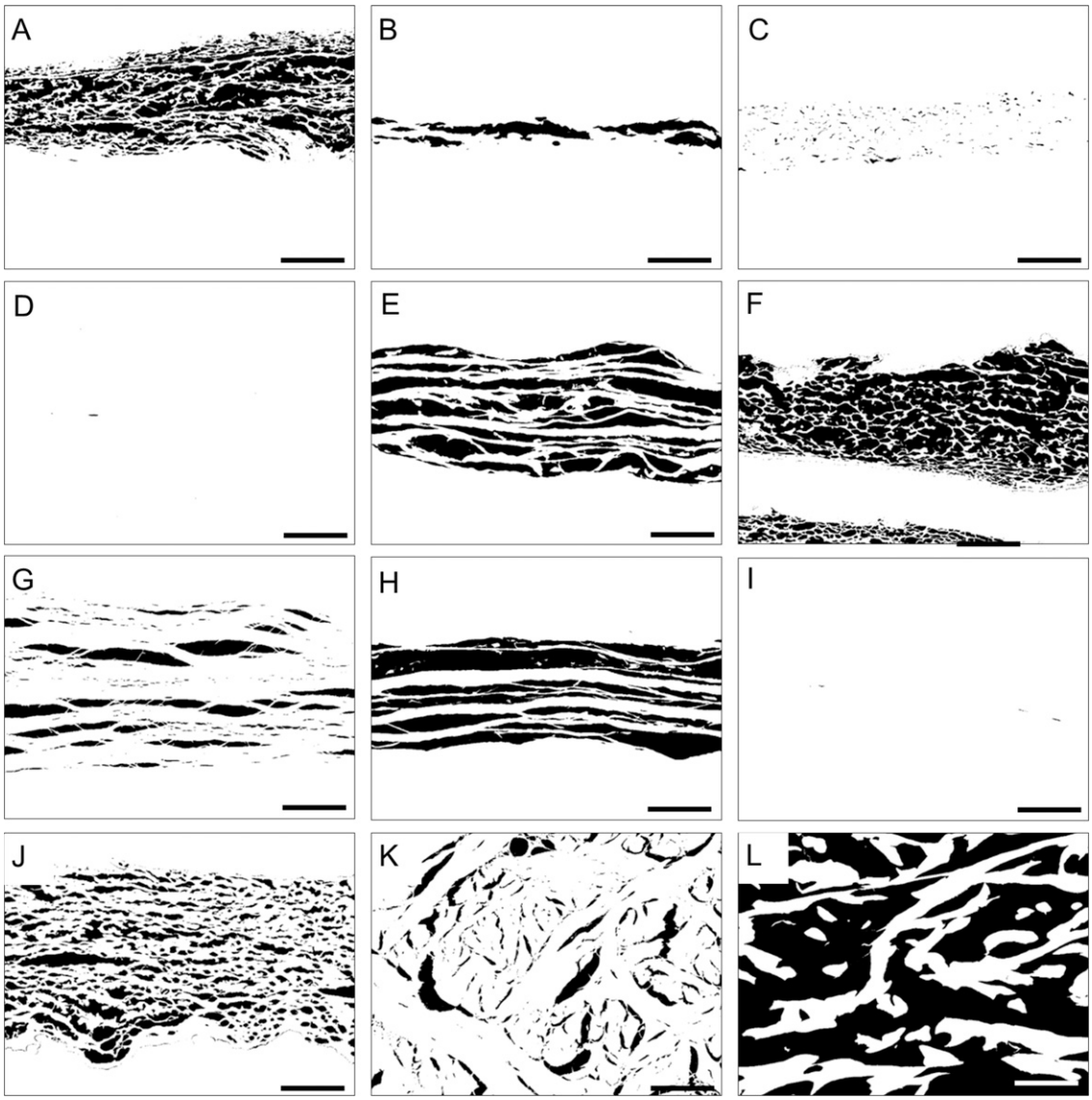

FIG. 4. Illustrative images of dermal and load bearing reconstruction products, where the *black* regions represent pores in each product sample. **(A)** OFMm; **(B)** PPN; **(C)** HDAM included as a minimally processed product; **(D)** PPC, **(E)** SISu; **(F)** OFMo; **(G)** UBM; **(H)** SISb; **(I)** SISz; **(J)** ADM; **(K)** PADM; **(L)** BADM. Scale bar = 100 μm.

the time of testing. Different applications have different requirements from a dECM repair scaffold, which is why it was deemed prudent to group materials based on their intended application, even if some were manufactured from the same type of tissue or technology. The manufacturing process required to laminate or strengthen a material can impact the native ECM structure, which is why such comparisons are important.

The scope of this study is limited to dermal reconstruction and load-bearing reconstruction procedures, however these test articles are also investigated for other applications, such as volumetric muscle loss, muscle flap reinforcement, and reconstructive surgery. Prior studies have concluded that biomaterials for soft tissue reconstruction perform optimally when they accurately mimic the native structure of tissue ECM with respect to collagen architecture, pore size distribution, and the presence of residual vascular channels.[36,37] However, the drive to retain native structure should not compromise the removal of cells or nuclear material that is known to lead to a negative host inflammatory response.[38]

While the source tissue is known to impact soft tissue regeneration with dECM materials,[39] the differences seen between products in this current study are likely heavily influenced not only by the source tissue but also by differences in the manufacturing process used for each product. Optimal tissue processing must strike a careful balance. Excessive tissue processing will effectively decellularize the tissue but can easily lead to damage of the protein architecture and loss of biological components that aid regeneration. Products that are minimally processed are likely to closely resemble the structure and composition of the source tissue but will contain a greater proportion of cells and cellular debris (e.g., HDAM, Fig. 2 and Fig. 6). These competing efforts have important

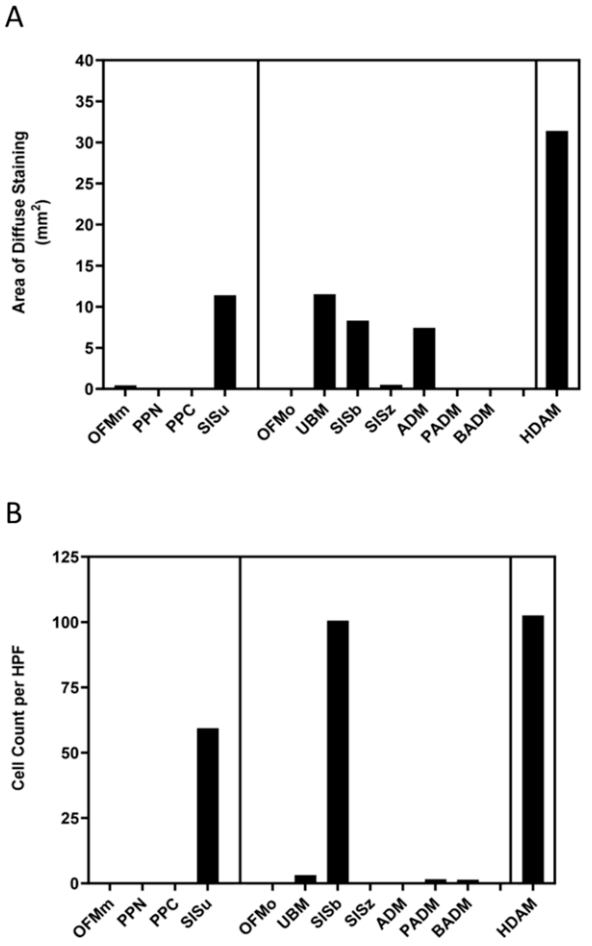

FIG. 5. Quantification of mean nuclear bodies per HPF **(A)** and mean area (mm^2) of diffuse staining per HPF **(B)** of product samples, based on DAPI stained sections. Results are expressed as mean from $n = 5$ HPF from a 1 cm^2 cross section of each material. HDAM is included as a minimally processed product. HDAM, human amnion/chorion.

clinical implications because they impact how host cells integrate into and remodel the products.

Soft tissue regeneration is a complex process that involves many cell types including fibroblasts, endothelial cells, keratinocytes, macrophages, lymphocytes, neutrophils, and progenitor cells. Biomaterial products are applied as "acellular" products and must be repopulated with host cells in order to integrate, remodel, and ultimately regenerate new well vascularized and functional tissue. Retaining the native interconnected structure and collagen organization of tissue ECM favors cell proliferation, vascularization, and subsequently, nutrient and oxygen supply to the defect site.[40] Cellular repopulation of the products contributes to the overall speed of healing via the capacity of host cells to adhere to the graft, migrate through the graft and proliferate. Porosity is a key determinant of the kinetics of these processes. *In vitro* studies on engineered porous materials have suggested "ideal" pore size ranges for various cell types. For instance, pore sizes between 90 and 130 μm have been demonstrated to permit fibroblast migration and proliferation.[41,42] A pore size ranging between 5 and 15 μm was shown to be beneficial for fibroblast ingrowth.[43] Furthermore, the pore sizes larger than 500 μm have been shown to facilitate the rapid vascularization of damaged tissue.[44] In this study, porosity was assessed qualitatively and was shown to vary considerably between different products. For example, the OFM products OFMm and OFMo scored highest for porosity based on pathological examination (Table 4) and demonstrate an open porous nature in inverted images (Fig. 4A and F). In contrast, PADM and SISz appear to have a very low level of porosity, appearing compacted (Fig. 4) and scored relatively low for porosity by pathology analysis (Table 4).

Previous *in vivo* studies have shown that the relative rates of cellular infiltration and tissue formation are directly proportional to the porosity assessment conducted herein. Overbeck *et al*. compared the relative cellular infiltration of commercial ECM-based products in a nonhuman primate model of hernia repair.[45] As would be predicted from our qualitative and quantitative assessment of porosity, the amount of early (4 weeks) cell infiltration was significantly higher in OFMo-treated animals compared with those treated with PADM or SISz.[45] This early infiltration of host cells may infer that the structural properties of OFMo such as pore size and collagen fiber organization are more amenable to cellular infiltration. Further evidence to support this is provided by the comparative *in vivo* study conducted by Overbeck *et al.*,[46] comparing OFMo with ADM in a primate model of hernia repair. This study demonstrated that cellular infiltration and ultimately device remodeling was faster in the OFMo group compared with the ADM group. This fate would be predicted when considering the relative porosity and collagen fiber organization (Table 4) of the two products.

The rate and quality of new blood vessel formation following graft repopulation is an important determinant of healing outcomes. It can be deduced that a material with a structure and porosity that is most amenable to new blood vessel formation is likely to perform better in a contaminated surgical environment. For example, several clinical studies have shown that the OFMm device is particularly resilient in a contaminated soft tissue defect.[47,48] The process of endothelial cell migration, vessel branching, and capillary development is a complex one, and influenced not only by the biological components of the device, but also structural features. Porosity is obviously a key criterion for endothelial cell migration. However, other structural features, such as residual vascular channels can aid neovascularization. The term "angioconduction" has been used to describe the process whereby host endothelial cells may use residual vascular channels present in a bioscaffold to template vascularization, akin to the structural features of bone grafts that enable osteoconduction.[25] The presence of residual vascular channels was qualitatively assessed from H&E-stained sections in the product samples (Table 4) and showed some variability. For example, the OFM-based devices, OFMm and OFMo, gave mean vascular channel scores of 1.00 ± 0.00 and 1.63 ± 0.52, respectively, even though these products comprise the same dECM material. Previous studies have shown that OFM-based devices lead to a greater *in vivo* number of blood vessels in a porcine full thickness excisional wound model versus SIS-based devices (e.g., SISb and SISz),[33] even though the SIS-based products scored relatively high for residual vascular channels (Table 4). This finding highlights that neovascularization within the products is driven by more than just

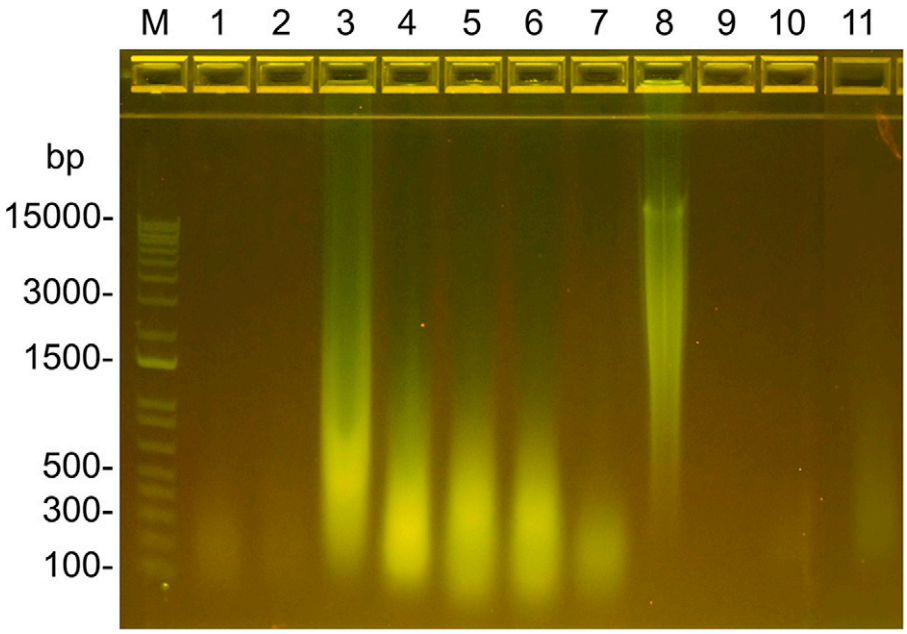

FIG. 6. Qualitative assessment of residual DNA by agarose gel electrophoresis. Lanes: **(M)** DNA marker; **(1)** OFM (representative sample of OFMm/OFMo); **(2)** PPN; **(3)** HDAM as a minimally processed product; **(4)** UBM; **(5)** SISu; **(6)** SISb; **(7)** SISz; **(8)** ADM; **(9)** PADM; **(10)** BADM; **(11)** PPC.

structural features (e.g., porosity and residual vascular channels) and the relative biological response from native signaling molecules also plays a critical role.

Effective decellularization is crucial for the removal of cellular and nuclear components from the source tissue, but must preserve the structural integrity and bioactive components of the dECM.[4] This includes the removal of intact cells as well as extracellular DNA, as measured by diffuse staining. Diffuse staining indicates cellular disruption but not removal of DNA. It is well known that removal of cellular, nuclear and cell lipid membrane components decreases the risk of a proinflammatory reaction *in vivo*.[49,50] HDAM was included in the panel as a minimally processed product, thus, complete removal of cellular bodies was not expected. Interestingly, while PADM and BADM show a low number of intact cells, ADM showed a high level of diffuse staining compared with PADM and BADM, indicating an effective method of cellular disruption but not removal or remnant DNA. OFMo, OFMm, PPC, and PPN were essentially devoid of nuclear material indicating that decellularization was appropriate, while maintaining ECM structure. Our results for PPN and PPC reflect previously published data describing the decellularization of these products.[51] The products SISu, SISb, SISz, and UBM showed a significant number of residual cellular bodies by DAPI-stained tissue sections (Figs. 2 and 3), pathology review (Table 4), and nuclear material by agarose gel (Fig. 7), indicating incomplete decellularization of the tissue. This is supported by findings that SIS materials retain matrix bound nanovesicles.[52] This potentially compromises clinical outcomes using these devices, as one would predict a proinflammatory (M1 macrophage phenotype) response based on the known biological response to xenogeneic nuclear material.[38] DNA or nuclear material "dosing" of ECM materials leads to a pronounced M1 macrophage response, causing scar tissue formation, encapsulation and seroma formation.[11] For example, one study[45] described outcomes of UBM in a primate model of hernia repair and showed graft loss, and fibrotic encapsulation 12 weeks postimplantation. As shown by the level of DNA in the materials tested (both animal and humanin origin) it is clear that a high degree or variability exists between materials. In addition, the amount of DNA a patient is exposed to will be subject to the type of procedure, and size of device used.

Table 3. Quantification of DAPI Fluorescence

Product sample	*Mean nuclear bodies per HPF*	*Area of diffuse staining per HPF (mm^2)*
OFMm	0.2 ± 0.5	0.4 ± 0.6
PPN	0.0 ± 0.0	0.0 ± 0.0
PPC	0.0 ± 0.0	0.0 ± 0.0
SISu	59.4 ± 7.5	11.4 ± 5.0
OFMo	0.2 ± 0.5	0.0 ± 0.0
UBM	3.2 ± 3.5	11.5 ± 4.3
SISb	101.8 ± 31.8	8.3 ± 3.3
SISz	0.3 ± 0.5	0.5 ± 0.6
ADM	0.0 ± 0.0	7.4 ± 2.6
PADM	1.5 ± 1.1	0.0 ± 0.0
BADM	1.7 ± 1.6	0.0 ± 0.1
HDAM	102.6 ± 17.6	6.9 ± 1.5

Results are expressed as the mean from assessment of five HPFs from a 1 cm^2 cross section per product. Errors represent standard deviation of the mean. Refer to supplementary materials for statistical analyses (Supplementary Table S1).

Based on the overall pathology score (Table 4), the products for dermal reconstruction could be ranked as follows: OFMm > PPC ≈ PPN > SISu. Similarly for the products intended for load-bearing applications, the overall pathology score ranked the products as follows: OFMo > PADM > BADM > ADM > UBM > SISb ≈ SISz. Interestingly, there are published clinical studies describing the relative performance of the devices, OFMo, PADM, and BADM in ventral hernia repair. Goetz *et al.*[53] retrospectively compared outcomes following surgical closure of contaminated ventral hernia with either OFMo, PADM, BADM, or Permacol™. Recurrence rates were significantly reduced in the OFMo group versus the comparator group (3.6% vs. 28.9%, respectively). A similar study comparing OFMo, PADM and BADM, reported hernia recurrence rates of

Table 4. Pathology Assessment

Product sample	*Collagen organization*	*Porosity*	*Cellular removal*	*Vascular channels*	*Overall score (out of 16)*
OFMm	2.5 ± 0.53	3.38 ± 0.52	3.63 ± 0.52	1.00 ± 0.00	10.5 ± 0.8
PPN	1.00 ± 0.00	1.00 ± 0.00	4.00 ± 0.00	1.00 ± 0.00	7.0 ± 0.0
PPC	1.00 ± 0.00	1.00 ± 0.00	4.00 ± 0.00	1.00 ± 0.00	7.0 ± 0.0
SISu	1.00 ± 0.00	1.50 ± 0.53	1.00 ± 0.00	1.13 ± 0.35	4.6 ± 0.5
OFMo	3.5 ± 0.53	3.88 ± 0.35	3.75 ± 0.46	1.63 ± 0.52	12.8 ± 1.0
UBM	1.38 ± 0.52	1.63 ± 0.52	1.00 ± 0.00	1.63 ± 0.52	5.6 ± 1.2
SISb	1.75 ± 0.46	1.88 ± 0.35	1.00 ± 0.00	1.25 ± 0.46	5.8 ± 0.6
SISz	1.00 ± 0.00	1.00 ± 0.00	1.25 ± 0.46	1.63 ± 0.52	4.9 ± 0.6
ADM	1.38 ± 0.52	2.00 ± 0.00	3.50 ± 0.53	1.38 ± 0.52	8.3 ± 0.5
PADM	2.88 ± 0.35	1.25 ± 0.46	3.88 ± 0.35	1.63 ± 0.52	9.6 ± 0.7
BADM	1.00 ± 0.00	2.75 ± 0.46	4.00 ± 0.00	1.00 ± 0.00	8.8 ± 0.5
HDAM	1.25 ± 0.46	1.63 ± 0.52	1.00 ± 0.00	1.00 ± 0.00	4.9 ± 0.8

Results are expressed as mean from the total pathology score (out of possible total score of 16) from eight HPFs from two cross sections per sample. Error bars represent standard deviation of the mean. Refer to supplementary materials for statistical analysis (Supplementary Table S2).

2.78%, 13.7%, and 24.3%, respectively.[54] In addition, the overall complication rates were also significantly reduced in the OFMo-treated cohort in comparison to the PADM and BADM cohorts (16.7%, 43.2%, and 47.1%, respectively).

Limitations

Although the most abundant tissue ECM proteins are structural collagens, a vast number of less abundant ECM components play significant roles in the mechanisms of tissue regeneration. It is the interplay between chemical and structural features of the ECM that facilitates processes such as tissue homeostasis, wound healing, and tissue regeneration. It is known that dECM products retain many of the biological components (e.g., growth factors) that naturally occur in tissue ECM.[30,55] This study was limited to structural and cellularity analysis of commercial products and did not evaluate the biological components, nor their associated biological or inflammatory response. This study did not explore the biophysical properties of the test articles as these have been published previously.[56] Biological materials are inherently heterogeneous, and variation can be expected from several sources, including: batch manufacturing process, tissue source (humans/animals—genetics, age, health), and regions of the organ a device is produced from. Quality control practices ensure that each device released meets predetermined limits. In this study, we compared multiple materials to provide a broad overview, assuming that batch-to-batch variation has been controlled or limited during the standardized manufacturing process.

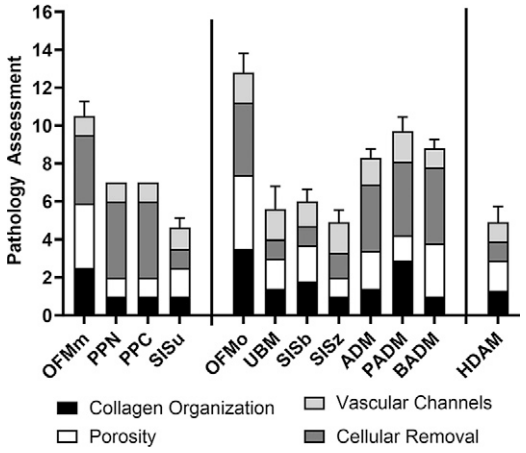

FIG. 7. Pathology assessment of dECM samples. Results are expressed as mean from the total pathology score (out of possible score of 16) of $n = 8$ HPFs. Error bars represent standard deviation. HPF, high-powered field.

Conclusions

The comparative analysis of commercially available dECM products revealed significant differences in the porosity of the bioscaffolds. While some products showed a porous structure that resembled the respective source tissue, other products showed little to no porosity. Furthermore, an analysis of nuclear staining demonstrated that the decellularization process used for several products was variable, suggesting these products may elicit a suboptimal inflammatory response. A comprehensive pathology assessment of all products demonstrated that OFMm, OFMo, and PADM scored best with respect to collagen fiber orientation/arrangement, matrix porosity, decellularization efficiency, and residual vascular channels. SISu and SISz scored poorly when assessed pathologically. Findings from this study may have implications for the clinical performance of these products.

Dedication

This article is dedicated to our late colleague and friend Dr. Maarten Persenaire who was always quick to share his wit and wisdom and always strove for a deeper understanding to improve patient outcomes.

Author Disclosure Statement

R.W.F.V., S.G.D., and B.C.H.M. are shareholders of Aroa Biosurgery Limited. T.K. and N.T. are/were employed by Aroa Biosurgery in the last 5 years.

Authors' Contributions

T.K.: writing—original draft; formal analysis; writing—review and editing. F.C.A.: formal analysis. R.W.F.V.: writing—review and editing. N.T.: writing—review and editing. V.M.v.H.: formal analysis; writing—review and editing. M.P.: supervision;

conceptualization. S.G.D.: supervision; conceptualization, formal analysis; writing—review and editing. B.C.H.M.: supervision; conceptualization; formal analysis; writing—review and editing; funding acquisition.

Funding Information

This research was undertaken by funding provided by Aroa Biosurgery and Callaghan Innovation Limited (New Zealand) Growth Grant (MSMA1402).

Supplementary Material

Supplementary Table S1
Supplementary Table S2

References

1. Powers JG, Higham C, Broussard K, et al. Wound healing and treating wounds: Chronic wound care and management. J Am Acad Dermatol 2016;74(4):607–625; doi: 10.1016/j.jaad.2015.08.070
2. Nicks BA, Ayello EA, Woo K, et al. Acute wound management: Revisiting the approach to assessment, irrigation, and closure considerations. Int J Emerg Med 2010;3(4):399–407.
3. Augustine R, Kalarikkal N, Thomas S. Advancement of wound care from grafts to bioengineered smart skin substitutes. Prog Biomater 2014;3(2–4):103–113; doi: 10.1007/s40204-014-0030-y
4. Heath DE. A review of decellularized extracellular matrix biomaterials for regenerative engineering applications. Regen Eng Transl Med 2019;5(2):155–166; doi: 10.1007/s40883-018-0080-0
5. Badylak S. The extracellular matrix as a scaffold for tissue reconstruction. Semin Cell Dev Biol 2002;13(5):377–383.
6. Bonnans C, Chou J, Werb Z. Remodelling the extracellular matrix in development and disease. Nat Rev Mol Cell Biol 2014;15(12):786–801; doi: 10.1038/nrm3904
7. Bosman FT, Stamenkovic I. Functional structure and composition of the extracellular matrix. J Pathol 2003;200(4):423–428; doi: 10.1002/path.1437
8. Badylak SF, Tullius R, Kokini K, et al. The use of xenogeneic small intestinal submucosa as a biomaterial for Achilles tendon repair in a dog model. J Biomed Mater Res 1995;29(8):977–985; doi: 10.1002/jbm.820290809
9. Hussey GS, Dziki JL, Badylak SF. Extracellular matrix-based materials for regenerative medicine. Nat Rev Mater 2018;3(7):159–173; doi: 10.1038/s41578-018-0023-x
10. Ezzelarab MB, Cooper DKC. Systemic inflammation in xenograft recipients (SIXR): A new paradigm in pig-to-primate xenotransplantation? Int J Surg 2015;23(Pt B):301–305; doi: 10.1016/j.ijsu.2015.07.643
11. Londono R, Dziki JL, Haljasmaa E, et al. The effect of cell debris within biologic scaffolds upon the macrophage response. J Biomed Mater Res A 2017;105(8):2109–2118; doi: 10.1002/jbm.a.36055
12. Cramer MC, Badylak SF. Extracellular matrix-based biomaterials and their influence upon cell behavior. Ann Biomed Eng 2020;48(7):2132–2153; doi: 10.1007/s10439-019-02408-9
13. Lynch K, Pei M. Age associated communication between cells and matrix: A potential impact on stem cell-based tissue regeneration strategies. Organogenesis 2014;10(3):289–298; doi: 10.4161/15476278.2014.970089
14. Kurtz A, Oh S-J. Age related changes of the extracellular matrix and stem cell maintenance. Prev Med 2012;54 Suppl:S50–S56; doi: 10.1016/j.ypmed.2012.01.003
15. Moriguchi T, Fujimoto D. Age-related changes in the content of the collagen crosslink, Pyridinoline1. J Biochem 1978;84(4):933–935; doi: 10.1093/oxfordjournals.jbchem.a132206
16. Yao Q, Zheng Y-W, Lan Q-H, et al. Recent development and biomedical applications of decellularized extracellular matrix biomaterials. Mater Sci Eng C Mater Biol Appl 2019;104:109942; doi: 10.1016/j.msec.2019.109942
17. Cheng CW, Solorio LD, Alsberg E. Decellularized tissue and cell-derived extracellular matrices as scaffolds for orthopaedic tissue engineering. Biotechnol Adv 2014;32(2):462–484; doi: 10.1016/j.biotechadv.2013.12.012
18. Song JS, Takimoto K, Jeon M, et al. Decellularized human dental pulp as a scaffold for regenerative endodontics. J Dent Res 2017;96(6):640–646; doi: 10.1177/0022034517693606
19. Yang B, Zhou L, Sun Z, et al. In vitro evaluation of the bioactive factors preserved in porcine small intestinal submucosa through cellular biological approaches. J Biomed Mater Res A 2010;93(3):1100–1109; doi: 10.1002/jbm.a.32534
20. Ueno T, Pickett LC, de la Fuente SG, et al. Clinical application of porcine small intestinal submucosa in the management of infected or potentially contaminated abdominal defects. J Gastrointest Surg 2004;8(1):109–112; doi: S1091255X03002257
21. Record RD, Hillegonds D, Simmons C, et al. In vivo degradation of 14C-labeled small intestinal submucosa (SIS) when used for urinary bladder repair. Biomaterials 2001;22(19):2653–2659; doi: S0142961201000072[pii]
22. Prevel CD, Eppley BL, Summerlin DJ, et al. Small intestinal submucosa: Utilization as a wound dressing in full-thickness rodent wounds. Ann Plast Surg 1995;35(4):381–388.
23. Lantz GC, Badylak SF, Hiles MC, et al. Small intestinal submucosa as a vascular graft: A review. J Invest Surg 1993;6(3):297–310.
24. Badylak SF, Lantz GC, Coffey A, et al. Small intestinal submucosa as a large diameter vascular graft in the dog. J Surg Res 1989;47(1):74–80; doi: 0022-4804(89)90050-4[pii]
25. Smith MJ, Dempsey SG, Veale RW, et al. Further structural characterization of ovine forestomach matrix and multi-layered extracellular matrix composites for soft tissue repair. J Biomater Appl 2021;36(6):996–1010; doi: 10.1177/08853282211045770
26. Raizman R, Hill R, Woo K. Prospective multicenter evaluation of an advanced extracellular matrix for wound management. Adv Skin Wound Care 2020;33(8):437–444; doi: 10.1097/01.ASW.0000667052.74087.d6
27. Melin M, Kaufman R, Geiger JEJ, et al. Clinical effectiveness of ovine forestomach matrix graft in complex lower limb reconstruction and limb salvage. Ottawa, Ontario, Canada.; 2023.
28. Lun S, Irvine SM, Johnson KD, et al. A functional extracellular matrix biomaterial derived from ovine forestomach. Biomaterials 2010;31(16):4517–4529; doi: 10.1016/j.biomaterials.2010.02.025
29. Howie Q, Longobardi J, Melin MM, et al. Clinical effectiveness of ovine forestomach matrix graft in complex lower limb reconstruction and limb salvage. Los Angeles, CA; 2022.
30. Dempsey SG, Miller CH, Schueler J, et al. A novel chemotactic factor derived from the extracellular matrix protein decorin recruits mesenchymal stromal cells *in vitro* and *in vivo*. PLoS One 2020;15(7):e0235784; doi: 10.1371/journal.pone.0235784

31. Dempsey SG, Miller CH, Hill RC, et al. Functional insights from the proteomic inventory of ovine forestomach matrix. J Proteome Res 2019;18(4):1657–1668; doi: 10.1021/acs.jproteome.8b00908
32. Al Mousa RH, Bosque BA, Dowling SG. Use of ovine forestomach matrix in the treatment of facial thermal burns. Wounds 2022;34(4):e17-21–eE21; doi: 10.25270/wnds/2022.e17e21
33. Irvine SM, Cayzer J, Todd EM, et al. Quantification of *in vitro* and *in vivo* angiogenesis stimulated by ovine forestomach matrix biomaterial. Biomaterials 2011;32(27):6351–6361; doi: l10.1016/j.biomaterials.2011.05.040
34. Sadtler K, Sommerfeld SD, Wolf MT, et al. Proteomic composition and immunomodulatory properties of urinary bladder matrix scaffolds in homeostasis and injury. Semin Immunol 2017;29:14–23; doi: 10.1016/j.smim.2017.05.002
35. Gu Y, Tang R, Gong DQ, et al. Reconstruction of the abdominal wall by using a combination of the human acellular dermal matrix implant and an interpositional omentum flap after extensive tumor resection in patients with abdominal wall neoplasm: A preliminary result. World J Gastroenterol 2008;14(5):752–757; doi: 10.3748/wjg.14.752
36. Guan Y, Liu S, Liu Y, et al. Porcine kidneys as a source of ECM scaffold for kidney regeneration. Mater Sci Eng C Mater Biol Appl 2015;56:451–456; doi: 10.1016/j.msec.2015.07.007
37. Swinehart IT, Badylak SF. Extracellular matrix bioscaffolds in tissue remodeling and morphogenesis. Dev Dyn 2016;245(3):351–360; doi: 10.1002/dvdy.24379
38. Brown BN, Valentin JE, Stewart-Akers AM, et al. Macrophage phenotype and remodeling outcomes in response to biologic scaffolds with and without a cellular component. Biomaterials 2009;30(8):1482–1491; doi: 10.1016/j.biomaterials.2008.11.040
39. Badylak SF. Decellularized allogeneic and xenogeneic tissue as a bioscaffold for regenerative medicine: Factors that influence the host response. Ann Biomed Eng 2014;42(7):1517–1527; doi: 10.1007/s10439-013-0963-7
40. Ebrahimi M. Porosity parameters in biomaterial science: Definition, impact, and challenges in tissue engineering. Front Mater Sci 2021;15(3):352–373; doi: 10.1007/s11706-021-0558-4
41. Yang Y, Zhu X, Cui W, et al. Electrospun composite mats of Poly[(D, L-lactide)-co-glycolide] and collagen with high porosity as potential scaffolds for skin tissue engineering. Macro Materials & Eng 2009;294(9):611–619; doi: 10.1002/mame.200900052
42. Chong EJ, Phan TT, Lim IJ, et al. Evaluation of electrospun PCL/gelatin nanofibrous scaffold for wound healing and layered dermal reconstitution. Acta Biomater 2007;3(3):321–330; doi: 10.1016/j.actbio.2007.01.002
43. Whang K, Healy KE, Elenz DR, et al. Engineering bone regeneration with bioabsorbable scaffolds with novel microarchitecture. Tissue Eng 1999;5(1):35–51; doi: 10.1089/ten.1999.5.35
44. Choi SW, Zhang Y, Macewan MR, et al. Neovascularization in biodegradable inverse opal scaffolds with uniform and precisely controlled pore sizes. Adv Healthc Mater 2013;2(1):145–154; doi: 10.1002/adhm.201200106
45. Overbeck N, Nagvajara GM, Ferzoco S, et al. In-vivo evaluation of a reinforced ovine biologic: A comparative study to available hernia mesh repair materials. Hernia 2020;24(6):1293–1306; doi: 10.1007/s10029-019-02119-z
46. Overbeck N, Beierschmitt A, May BCH, et al. In-Vivo evaluation of a reinforced ovine biologic for plastic and reconstructive procedures in a non-human primate model of soft tissue repair. ePlasty 2022;22(e43).
47. Bosque BA, Dowling SG, May BCH, et al. Ovine forestomach matrix in the surgical management of complex lower-extremity soft-tissue defects: A retrospective multi-center case series. J Am Podiatr Med Assoc 2023;113(3):22–81; doi: 10.7547/22-081
48. Cormican MT, Creel NJ, Bosque BA, et al. Ovine forestomach matrix in the surgical management of complex volumetric soft tissue defects: A retrospective pilot case series. ePlasty 2023;23:e66.
49. Gilbert TW, Sellaro TL, Badylak SF. Decellularization of tissues and organs. Biomaterials 2006;27(19):3675–3683; doi: 10.1016/j.biomaterials.2006.02.014
50. Parmaksiz M, Elcin AE, Elcin YM. Decellularization of bovine small intestinal submucosa and its use for the healing of a critical-sized full-thickness skin defect, alone and in combination with stem cells, in a small rodent model. J Tissue Eng Regen Med 2017;11(6):1754–1765; doi: 10.1002/term.2071
51. Capella-Monsonís H, Tilbury MA, Wall JG, et al. Porcine mesothelium matrix as a biomaterial for wound healing applications. Mater Today Bio 2020;7:100057; doi: 10.1016/j.mtbio.2020.100057
52. Huleihel L, Hussey GS, Naranjo JD, et al. Matrix-bound nanovesicles within ECM bioscaffolds. Sci Adv 2016;2(6):e1600502; doi: 10.1126/sciadv.1600502
53. Goetz M, Jurczyk M, Junger H, et al. Semiresorbable biologic hybrid meshes for ventral abdominal hernia repair in potentially contaminated settings: Lower risk of recurrence. Updates Surg 2022;74(6):1995–2001; doi: 10.1007/s13304-022-01378-3
54. Sivaraj D, Henn D, Fischer KS, et al. Reinforced biologic mesh reduces postoperative complications compared to biologic mesh after ventral hernia repair. Plast Reconstr Surg Glob Open 2022;10(2):e4083; doi: 10.1097/GOX.0000000000004083
55. Marçal H, Ahmed T, Badylak SF, et al. A comprehensive protein expression profile of extracellular matrix biomaterial derived from porcine urinary bladder. Regen Med 2012;7(2):159–166.
56. Deeken CR, Lake SP. Mechanical properties of the abdominal wall and biomaterials utilized for hernia repair. J Mech Behav Biomed Mater 2017;74:411–427.

Address correspondence to:
Sandi G. Dempsey, PhD
Aroa Biosurgery Limited
64 Richard Pearse Drive
Auckland 2022
New Zealand

E-mail: sandi.dempsey@aroa.com

Received: February 22, 2024
Accepted: July 18, 2024
Online Publication Date: September 14, 2024